applied sciences

MDPI

Article

Mechanical Characterization of a Polymer/Natural Fibers/Bentonite Composite Material with Implementation of a Continuous Damage Model

Meylí Valin Fernández [1,*], José Luis Valin Rivera [2], Frank Pérez Rodríguez [3], Henry Figueredo Losada [4], María Elena Fernández Abreu [2], Francisco Rolando Valenzuela Diaz [5], Angel Rodríguez Soto [2], Alexander Alfonso Alvarez [6], Roberto Quinteros [2], Cristobal Galleguillos Ketterer [2] and Gilberto García del Pino [7]

1 Department of Mechanical Engineering (DIM), Faculty of Engineering (FI), University of Concepción, Concepción 4030000, Chile
2 Escuela de Ingeniería Mecánica, Pontificia Universidad Católica de Valparaíso, Valparaíso 2340025, Chile
3 Departamento de Tecnología de Construcción de Maquinarias (TCM), Facultad de Ingeniería Mecánica, Universidad Tecnológica de La Habana (Cujae), La Habana 19390, Cuba
4 Departamento de Diseño Mecánico, Instituto de Ingeniería Mecánica y Producción Industrial (IIMPI), Facultad de Ingeniería, Universidad de la República, Montevideo 11200, Uruguay
5 Departamento de Engenharia Metalúrgica e de Materiais, Escola Politécnica da Universidade de São Paulo, Universidade de São Paulo, USP, São Paulo 05508-220, Brazil
6 Departamento de Ingeniería Mecánica, Facultad de Ingeniería, Universidad de la Serena, La Serena 1720010, Chile
7 College of Technology, State University of Amazonas, Manaus 69850-000, Brazil
* Correspondence: mvalin@udec.cl

Abstract: A characterization of composite materials of a polyester matrix reinforced with natural fibers of Cuban henequen and organophilized Cuban bentonite was carried out, the experimental results of which are used to formulate, implement, and validate a scalar damage model. The fibers were added on a weight basis of 15, 20, and 25% as a reinforcing material, and organophilized Cuban bentonite, in amounts of 3, 5, and 7% by weight, was added. Samples containing only polymer and fibers showed the best mechanical performance for 25% of fiber, with increases of 51% in the tensile strength and 169% on the impact resistance. Samples containing polymer and clay showed the best results for 5% of bentonite, with increases of 89% in the tensile strength and 83% on the impact resistance, and samples containing 25% fiber and 5% clay were also prepared and achieved a 98% increase in the tensile strength and 219% in the impact strength. The scalar damage model deals with an internal variable, which corresponds to the damage variable, together with a failure surface that allows identifying the mechanical state of the material dependent on the mechanical stress, obtaining an adequate correlation with the results of the experimental tests.

Keywords: composite; natural fibers; mechanical properties; damage model

Citation: Fernández, M.V.; Rivera, J.L.V.; Rodríguez, F.P.; Losada, H.F.; Abreu, M.E.F.; Diaz, F.R.V.; Soto, A.R.; Alvarez, A.A.; Quinteros, R.; Ketterer, C.G.; et al. Mechanical Characterization of a Polymer/Natural Fibers/Bentonite Composite Material with Implementation of a Continuous Damage Model. *Appl. Sci.* **2023**, *13*, 2677. https://doi.org/10.3390/app13042677

Academic Editor: Aimin Yu

Received: 21 January 2023
Revised: 15 February 2023
Accepted: 17 February 2023
Published: 19 February 2023

1. Introduction

The development of polymeric composites reinforced with natural fibers, such as jute, henequen, coconut, linen, and others is an alternative to synthetic fibers, based on abundance, biodegradability, low weight, toxicity, and low cost of application compared to synthetic fibers [1–4]. Vegetable fibers are less abrasive than inorganic fibers, usually used as a reinforcement, and thus generate less wear in the equipment involved in its processing [5–7]. In addition, they have good mechanical properties; for example, Hossen et al. [8] evaluated the tensile strength properties of a composite formed by jute fiber with thermoplastic polymer granules 3 mm in length used as the matrix material and a montmorillonite clay surface modified with 25–30 wt% octadecylamine (Nanoclay, Nanomer®

I.30E), and observed an increment in the tensile strength of 20% for a 15% addition of fiber, compared to the material without fibers. According to [9], a specimen prepared by a hand layup technique with jute (20 wt%), hemp (20 wt%), sisal (20 wt%), and glass fibers (30 wt%) with Epoxy LY-556 matrix (50 wt%), presented a tensile strength of 75.2 MPa and a flexural strength of 95.4 MPa. On the other hand, ref. [10] studied a biocomposite of polypropylene as a matrix, using hemp fibers with an average length and diameter of 7 ± 0.5 cm and 25 ± 5 µm, respectively, as the reinforcement after undergoing a special chemical treatment, and polypropylene grafted with maleic anhydride as the coupling agent. An increase of the Young's modulus from 0.85 GPa to 2.12 GPa for the reinforced with 30wt% hemp fibers representing an increase of 149% was founded. The flexural modulus was increased by 46%, 165%, and 232% compared to the matrix without fibers for an addition of 10, 30, and 40%; this represents flexural strength increases of 52%, 78%, and 92% relative to the matrix for a 10, 30, and 40% addition of fiber [10]. Moreover, Mylsamy et al. report an increase in the tensile, flexural, and impact strength in samples with Coccinia Indica fiber fabricated via compression molding with maximum values for 30 mm in the fiber length and 35% weight for the ratios for the fiber loading [11].

Particles have also been used as reinforcements in polymer and polyester matrices, as presented by Kumar, which studied the effect of nanoclay particles on the mechanical properties of a composite of polyester resin reinforced with vakka fiber. Vakka fibers were cut into lengths of 160 mm and mixed with ECMALON 4413 grade polyester resin using the hand layup technique with a maximum volume fraction of fiber limited to 0.40 because sample delamination takes place with higher volume fractions. The results showed that the strength and flexural strength are 21.2% and 55% higher than the composites without the addition of nanoclay at a 45% volume fraction [12]. Likewise, Ranjith reports a study of a composite with epoxy (LY556), hardener (HY951), nanoclay (25%), and multiwall carbon nanotube (25%) manufactured using the vacuum bag process where the last one was used were used as a filler material to test their influence on the flexural properties of a glass fiber [13]. On the other hand, bentonite (Sigma Aldrich, St. Louis, MO, USA) and ethyl cellulose ($[C_6H_7O_2(OH)_{3-x}(OC_2H_5)_x]n$, Hercules, USA) with an ethyl group content of 48%, substitution degree of 2.8, and viscosity of 7 cP were used by Alekseeva et al. to prepare polymer/clay composites. The bentonite-modified polymer film samples presented a growth in the tensile strength of 207.5, 140, and 150 MPa, for a 0.5, 1, and 3–5 weight for the ratios of bentonite in comparison with those of pure ethyl cellulose 144 MPa [14].

In the construction area, some studies have been developed, as was presented by [15] where a fiber-reinforced polymer mesh was applied on the faces of a masonry wall, embedded in a mortar layer with a nominal thickness of 30 mm, and a numerical model was developed. Rashmi et al. [16], on the other hand, compared the behavior of the natural fibers of jute and sisal, compared to the polypropylene fiber in cement, cement-lime and cement-APA (air entraining plasticizer admixture) mortars. Finding that, at higher percentages of natural fiber up to 2%, the resistance is affected, this was attributed to an increase in the porosity of the material compared to the reference material. Concrete beams strengthened with an ultra-rapid-hardening fiber-reinforced mortar were investigated by [17] and increases of 11% in the flexural strength and 15% in the toughness were found. Meanwhile, Silva et al. [18] report the use of natural fibers as pineapple leaf, sisal, linen, and others, as aggregates of ordinary concrete, highlighting their benefits.

These materials have a potential application as masonry structures, and previous works [19–21] used sisal fibers as sustainable materials for construction, as well as structural health monitoring applications [22] and electrical insulation [23]. All this speaks about the several applications and uses of natural and synthetic fibers in structures, considering not only their benefits in mechanical properties, but also their characteristics of thermal and acoustic insulation and biodegradability.

Despite this, the design of composite structures is quite conservative in engineering practice as it is expensive and time-consuming, and many tests must be performed to ensure the safety of the structures [24]. Therefore, the mechanics of continuous damage

play an important role in the design, production, and health control of composite structures, through the study of the criteria of discontinuity, accumulation of damage, softening of properties, etc. [25].

The damage of a material is caused by a reduction in the area, due to the generation of cracks or discontinuities, which implies a decrease in the ability to resist efforts as the stresses increase [26]. A continuous damage model does not attempt to describe what happens at the point where such discontinuity is caused, but rather is governed by the basic hypothesis of obtaining a global response from the structure affected by the phenomenon of the fracture, through constitutive equations and damage evolution based on irreversible thermodynamic processes, together with the theory of internal state variables [26]. Moreover, a hybrid model was proposed by Rezasefat et al. to analyze the resin-rich uncertainty in the composite material. The discretization window size was mitigated using microstructure images and point-to-point mapping for the estimation of the mechanical properties [27]. Tijs et al. investigated the ability of continuous damage models to accurately predict the matrix failure and layer splitting. He used two approaches, one based on incremental small strain increments and Cauchy stress, and another approach that takes strain kinematics into account by using Green–Lagrange strain and Piola–Kirchhoff second stress [28].

In this paper, we aim to establish a failure criterion for continuous damage for a thermostable polymer matrix verifying the influence of the mass of henequen fibers, as the reinforcement, on the mechanical properties, considering that the propagation of aggregation and nucleation does not produce an instantaneous collapse of the matrix or rapid structural collapse, since the transverse microcracks of the matrix produce an intralaminar failure, which degrades the mechanical properties of the material gradually and gradually until its total collapse is presented.

2. Materials and Methods

2.1. Simplified Outline of the Investigation

The present work entailed the characterization of compounds and the elaboration of a numerical model through a series of steps whose synthesized scheme is presented in Figure 1.

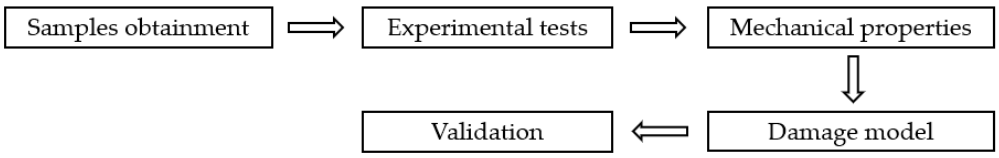

Figure 1. Outline of the investigation.

2.2. Materials

The resin used was formed by a homogeneous, polyester-based, central polymer chain compound dissolved in styrene monomer. It works as the resin diluent but also has a structural function in curing the resin. Another component of the resin is an inhibitor, which allows it to not react spontaneously; it means that the resin does not cure prior to the aggregation of the promoters of the reaction. For the development of this research, pure orthophthalic polyester resin (thermostable), produced by Lonza Group Co., under the trade name Distitron 5119, was used and whose characteristics and values are shown in Table 1 and Figure 2, respectively.

Table 1. Data of the polyester Distitron 5119.

Properties	Test Methods	Typical Values
Color	RS13F	light yellow
Odor	-	styrene
Acid number	RS02	24–31 mg KOH/g
Stability at 20 °C in the dark	RS07G	six months
Apparent density	ISO 2811	1.1–1.15 g/cm^3
RVF viscosity, s 2 rpm	GM025	580–700 mPa.s
Styrene monomer content	RS06C	31–35%
Reactivity	0.3%Co6% + 0.8%MEKP	
Gel time	RS13G	20–26 min.
Hardening time	RS13G	31–43 min.
Exothermic peak	RS13G	140–170 °C
Flashpoint	EN 22719	31 °C

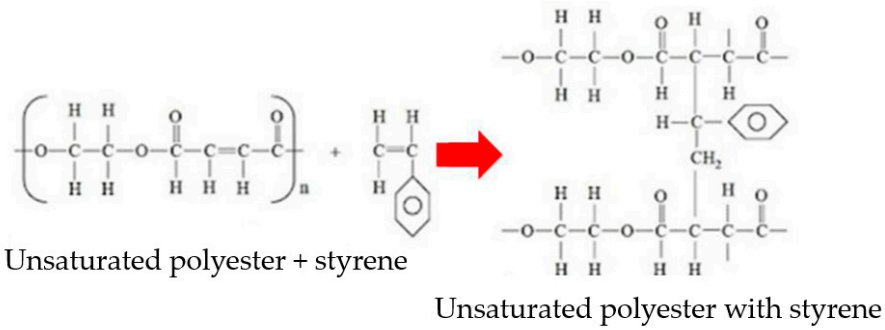

Figure 2. Obtaining unsaturated polyester with styrene.

The catalyst used was Curox M-302 (methyl ethyl ketone peroxide) produced by United Initiators GmbH, in the ratio of 2.0%, whose characteristics and values are shown in Table 2 and Figure 3, respectively.

Table 2. Data of the Curox M-302.

Properties	Typical Values
Physical state and color	liquid and colorless
CAS number	1338-23-4
Formula	$C_4H_{10}O_4$
Flashpoint	56°C, Method: ISO 3679, Seta–Flash.
Melting point/range	−10 to −5.5 °C
Vapor pressure	0.184 Pa at 25 °C
Density	1.02 g/cm^3 at 20 °C
Water solubility	Approximately 6.5 g/L at 20 °C
Dynamic viscosity	13 mPa.s at 20 °C
Refractive index	1.43 at 20 °C

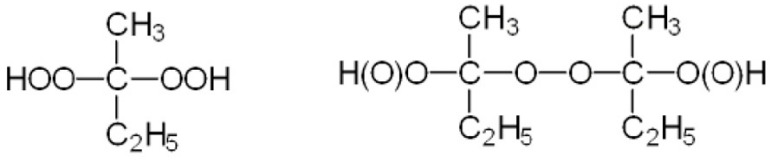

Figure 3. Methyl-ethyl-ketone peroxide formula.

This unsaturated polyester was chosen for its properties and its versatility, since it can be used as binding resins to make highly resistant synthetic fibers, transparent films, corrugated sheets, varnishes, and protective paints. On the other hand, this polymer, thanks to its properties and its sintering mode, gave us the possibility of simple processing by manual molding of the compound without the need for heat administration or the presence of a cooling system, as well as a relatively short natural cure time.

As the reinforcing component, the Henequén fiber from Cuba (Agave fourcroydes), from Limonar, Matanzas Province, Cuba, was used. The optimum length was determined according to the critical length criterion, as presented by Equation (1).

$$l_c = \frac{\sigma_f d_f}{2\tau_c} \tag{1}$$

where l_c is the critical length, σ_f is the maximum stress that the fiber resists, d_f is the fiber diameter, and τ_c is the shear strength of the matrix.

The fibers were tested in a TA HD PLUS machine, brand-Stable Micro System with a capacity of up to 250 kgf, with controlled temperature and humidity of 250 °C and 60 RH. Measurements were taken on a total of 20 fibers, which were each cut in two and tests were carried out on both halves, taking the average of the results for each fiber and an average for the total fibers measured. The 20 fibers used as test bodies in the tensile breaking strength test were determined by their cross-sectional area (A_t), by means of Equation (2), since their geometry is close to a circular section, which depends on its diameter (d_f). The cross-section of the fiber was measured using a Carl Zeiss Jena optical microscope at 100× coupled to a computer.

$$A_t = \frac{\pi {d_f}^2}{4} \tag{2}$$

The average values of the fiber diameter and the maximum stress that it resists were 0.32 mm and 270.07 MPa, respectively. The shear limit values of the matrix τ_c were obtained through mechanical tests performed on cylindrical polymer samples, with a diameter of 10 mm and an area of 78,54 mm^2, with an average value of 9.61 MPa. Substituting in Equation (1), we obtained the critical length of 35 mm. For values less than the one obtained, the action of the reinforcement in the composite material is not effective. For this reason, it was decided to take a value of 80 mm to obtain the composite material developed in our research. The fibers were weighed to ensure the reinforcement of 15, 20, and 25% on a weight basis. This weight was determined on the basis of the mass of a polymer plate and henequen fiber. Furthermore, as a reinforcing material, in relation to the amount of fibers used, a certain proportion of organophilized bentonite was added. The fibers were cut using a BCL 1309X model laser from the BODOR company with an intensity of 10 (mA) and a cutting speed of 14 mm/s at a distance of 3 mm from the nozzle of the machine to the surface of the fiber to be cut.

The organophilized calcium bentonite was modified with sodium carbonate (110 meq/100g dry clay) and with quaternary ammonium salt (QUAT) hexadecyl trimethyl ammonium chloride, which was added to the hydrated suspension containing 100 meq of bentonite/100g of clay (25.6 g QUAT—40 g of clay). The clay was decanted, washed, dried, and crushed (passing through the ABNT 200 sieve–0.075 mm aperture) before use. The molding release material used was Meltonian, Boot Shoe Cream Polish, number 6 Light Brown Brun Clair, product manufactured in the United States of America.

2.3. Characterization

After blending fibers and polyester resin, and before the resin reached its gelling point, the mold was closed and placed in the press, where 5 t pressing was applied for 4 h at room temperature. It was decided to use this pressing value due to its reference in previous works, in which good results have been achieved in the manufacture of the composite material [7,29,30].

In another stage of the work, samples of composite material were prepared in the proportions of 3, 5, and 7% m/m of clay (organophilic bentonite) in addition to the polymer to evaluate the concentration of clay with which to obtain the best results for its mechanical properties. The clay was first added to the resin, then manual homogenization was performed with glass stick and proceeded as above. The samples obtained, as well as their composition, are shown in Table 3.

Table 3. Denomination and composition of the prepared samples.

Sample	Fiber [%]	Bentonite [%]
PoS	-	-
PoH15	15	-
PoH20	20	-
PoH25	25	-
PoB3	-	3
PoB5	-	5
PoB7	-	7
PoB5H15	15	5
PoB5H20	20	5
PoB5H25	25	5

The samples covered with gold were examined in the Philips XR-30 scanning electron microscope of the Department of Metallurgical Engineering and Materials of the Polytechnic School of the University of São Paulo, Brazil. A polymer sample containing 5% bentonite and 25% fiber was examined using the JEOL 1010 Electronic Transmission Microscope by JEOL (Peabody, MA, USA, Solutions for innovation) company of USA.

For the characterization of the materials manufactured, the following tests were carried out: traction, following the Standard Test Method for Tensile Properties of Polymer Matrix Composite Materials (ASTM D 3039), and impact, following the Standard Test Methods for Determining the Izod Pendulum Impact Resistance of Plastic (ASTM D 256). The dimensions of the test samples were 3 mm thick, 250 mm long, and 30 mm wide for the tensile test and 3 mm thick, 63.5 mm long, and 12.7 mm wide for the impact test, as shown in Figure 4. The tensile test was performed using the IBERTEST universal testing machine, with local temperature 25 °C, controlled constant humidity of 60%, and velocity of 0.1 m/s. The impact test was performed on the Time Group Inc. (Beijing, China) XJU-22 impact machine, proof type: Izod impact, 5 kg-m power; 50 J (Joule).

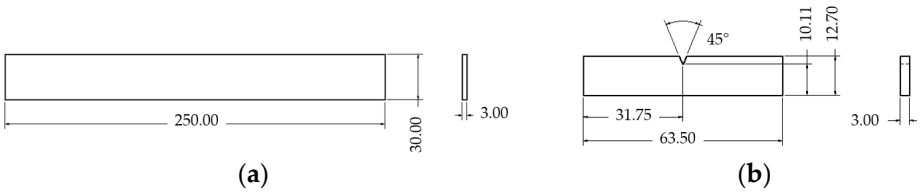

Figure 4. Dimension and shape of samples. (**a**) Tensile test and (**b**) impact test.

2.4. Computational Model

The constitutive model is based on the damage evolution rule from a tensile failure surface and the definition of the scalar damage parameter, according to four material parameters. These are defined from the different properties determined in a tension-

displacement test, implemented in the commercial software ABAQUS (Simulia D.S., 2014) by means of a subroutine with explicit VUMAT integration.

A single scalar variable, d, that affects all the components of the tensor equally maintaining isotropy conditions [31,32], was proposed once the damage starts with respect to the Hashin criterion, that does not violate the first and second laws of thermodynamics [24]. The damage variable had a domain of [0, 1], with value 1 for not damaged, and value 0 for completely damaged. The stress tensor expressed is presented in Equation (3), where σ_{ij} is the stress tensor of the real space, $\overline{\sigma}_{ij}$ the effective stress tensor or the undamaged space, C^0_{ijkl} the elastic constitutive tensor, ε_{kl} the deformation tensor, and d the damage variable, according to [31]. The validation was obtained from the contrast with the results obtained in the experimental tests, according to the ASTM D3039 standard for the case of an element subjected to increasing axial traction.

$$\sigma_{ij} = (1-d)\overline{\sigma}_{ij} = (1-d)C^0_{ijkl}\varepsilon_{kl} \tag{3}$$

A linear elastic model was implemented that satisfies the following stability conditions: Equilibrium condition

$$\frac{\partial \sigma_{ij}}{\partial x_j} = -\rho b_i \tag{4}$$

Equilibrium condition on the boundary

$$\sigma \cdot n = t \tag{5}$$

Infinitesimal strain condition

$$\varepsilon_{ij} = \frac{1}{2}\left(\frac{\partial u_i}{\partial x_j} + \frac{\partial u_j}{\partial x_i}\right) \tag{6}$$

The linear relationship such as the generalized Hooke's law meets these conditions and is presented in Equation (7).

$$\sigma_{ij} = C_{ijkl}\varepsilon_{kl} \tag{7}$$

The constitutive fourth order tensor, C_{ijkl}, has only two independent terms, which are Young's modulus, E and the Poisson's ratio, v, and was used only in the zone of elastic behavior as presented in Equation (8) where μ and λ are the Lame's constants.

$$\sigma_{ij} = \mu\varepsilon_{ij} + \lambda\varepsilon_{kk}\delta_{ij} \tag{8}$$

For the model to have physical and numerical stability, the Drucker criterion was used, while the stability condition is guaranteed if the Hessian is definitively positive [33].

$$H_{ijkl} = \mathbf{H} = det\left|\frac{\partial^2 \Psi(\varepsilon)}{\partial\varepsilon \otimes \partial\varepsilon}\right| > 0 \tag{9}$$

The implemented continuous damage model begins when the discontinuity criterion is satisfied, based on a scalar function of tensor arguments that delimits the elastic domain. In this way, the main objective of this model is to reduce the properties of the stiffness matrix, in response to the loss of properties, since different studies affirm that composite materials present a subcritical damage prior to the total damage of the material. On the other hand, the criterion for the onset of damage, according to the physical nature of the model, is presented in Equation (10), which allowed evaluating the effective tension in the longitudinal direction when it is in tension ($\overline{\sigma}_{11} > 0$), where X_T is the tensile strength in the direction of the fibers.

$$e_{ft} = \left(\frac{\overline{\sigma}_{11}}{X_T}\right)^2 \tag{10}$$

The model complies with the laws of thermodynamics under the implicit assumption of small deformations, which implies that the density of the material (ρ) can be considered constant [24,34–37]. The Clausius–Duhem inequality [35], or dissipation inequality, was decomposed into a mechanical and thermal part. Using the Gibbs free energy and the Legendre transformation the energy under a dependence of the internal variables of the model was introduced. Through the study of Coleman and Noll [36,37], and considering that the temperature is uniformly distributed ($\gamma_{term} = 0$), the dissipation inequality is presented as Equation (11), where γ is the power dissipated per unit volume decomposed into a mechanical and thermal part and (h) is the internal variable of the model.

$$\gamma = \gamma_{mec} + \gamma_{term} = -\rho \frac{d\phi}{dh} \dot{h} > 0 \tag{11}$$

The damage variable used is presented in Equation (12), where the variables are the components of the equivalent stress and equivalent strain.

$$\sigma_{eq} = \frac{\sigma_{eq}^{0}}{\varepsilon_{eq}^{0} - \varepsilon_{eq}^{f}} \varepsilon_{eq} + \frac{\varepsilon_{eq}^{f} \sigma_{eq}^{0}}{\varepsilon_{eq}^{f} - \varepsilon_{eq}^{0}} \tag{12}$$

Considering $\sigma_{eq} = d\overline{\sigma}_{eq}$, the damage parameter, for whatever failure mode is presented as Equation (13).

$$d_t = \frac{\sigma_{eq-t}^{0}}{E_{eq-t}\left(\varepsilon_{eq-t}^{0} - \varepsilon_{eq-t}^{f}\right)} + \frac{\varepsilon_{eq-t}^{f} \sigma_{eq-t}^{0}}{E_{eq-t}\left(\varepsilon_{eq-t}^{f} - \varepsilon_{eq-t}^{0}\right)} \frac{1}{\varepsilon_{eq-t}} \tag{13}$$

In the proposed model, the method carries out the analysis using time increments, that is, iterations are not required to obtain the solution of the equation, since it updates the accelerations, velocities, and displacements. The type of element used was the tetrahedral CD8RD with a characteristic length of Lc = 1.0 mm. Therefore, in the numerical simulations, there is no local failure when applying a point load, and a unidirectional displacement imposed on one of the ends of the specimen is proposed, as illustrated in Figure 5. In the area where the displacement is imposed, a boundary condition is established that limits the rotation and linear movement in the axis perpendicular to the imposed deformation, which corresponds to the z axis.

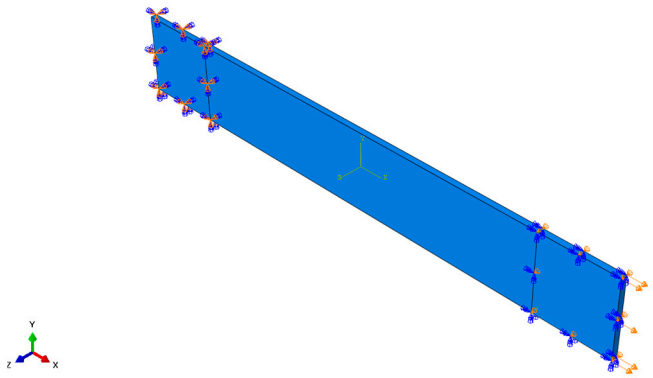

Figure 5. Boundary conditions in the computational model.

The numerical simulation is based on the implementation of an explicit integration rule together with the use of mass matrices of diagonal elements or groups. This method, to find the solution U^{+t}, carries out the analysis using time increments, that is, no iterations are required to obtain the solution of the equation since it updates the accelerations, velocities, and displacements. Such updates of the acceleration, velocity, and displacement vectors are performed at each time increment. At the beginning of each time increment, the software

calls a subroutine and returns the strain tensor. In this way, the code uses this tensor to update the state variables, d and τ (damage and damage threshold), and with them the stress tensor, σ_{ij}, to deliver it to the software. One of the advantages of explicit analysis is the computational efficiency of the process, since it uses the diagonal mass shader, which facilitates its inversion at the beginning of the triaxial increment.

In the sequence below, the pseudocode of the proposed calculation is presented.

1. Abaqus returns, at the start of the increment, the incremental strain tensor, $\Delta\varepsilon$.
2. With the increase in strain, the algorithm calculates the strain tensor, and the effective stress tensor.

$$\varepsilon^{(t+1)} = \varepsilon^{(t)} + \Delta\varepsilon^{(t+1)} \tag{14}$$

3. The damage variables, d, and damage threshold, r, are updated, respectively.
4. The effective effort is calculated.

$$\overline{\sigma}^{(t+1)} = \sigma^{(t)} M^{-1} + \varepsilon^{(t+1)} \tag{15}$$

and the conjugate thermodynamic force of the damage variable

$$Y^{(t+1)}\left(\psi^0\right) = \frac{1}{2}\varepsilon_{ij}^{(t+1)} C_{ijkl}^0 \varepsilon_{kl}^{(t+1)} \tag{16}$$

5. Verification of damage criteria.

$$\text{If g}\left(\overline{\tau}^{(t+1)}, r^{(t+1)}\right) < 0 \text{ elastic behavior} \tag{17}$$

$$\text{If g}\left(\overline{\tau}^{(t+1)}, r^{(t+1)}\right) > 0 \tag{18}$$

- Damage evolution $d^{(t+1)} = G\overline{\tau}^{(t)}$.
- Damage threshold update $r^{(t+1)} = \overline{\tau}^{(t+1)}$

6. Update of the tension tensor, to deliver them to Abaqus.

$$\sigma_{ij}^{(t+1)} = \left(1 - d^{(t+1)}\right) I_{ijkl} C_{ijkl}^0 \varepsilon_{kl}^{(t+1)} \tag{19}$$

7. End of the process of explicit integration of the constitutive equation.

3. Results

3.1. Characterization Results

The results obtained in the tests of the tensile strength of the matrix and of the polymer/fiber composites (15, 20, and 25%) are shown in Figure 6a. A positive influence of the henequen fiber was observed when mixing with the polymer, resulting in increments in the tensile strength where the highest value (24.2 MPa) was obtained with the composite containing 25% fiber. The increases are due, not only to the high mechanical strength of the henequen fibers [38] when compared with other natural fibers [39], but also to the surface with an irregular texture that shows grooves in the longitudinal sense of the fibers. In addition, it is observed in Figure 7 that the resin occupies the recesses of the fiber, taking its shape, thus causing, besides the interfacial forces, a mechanical adherence that contributed to the increases in the tensile strength obtained.

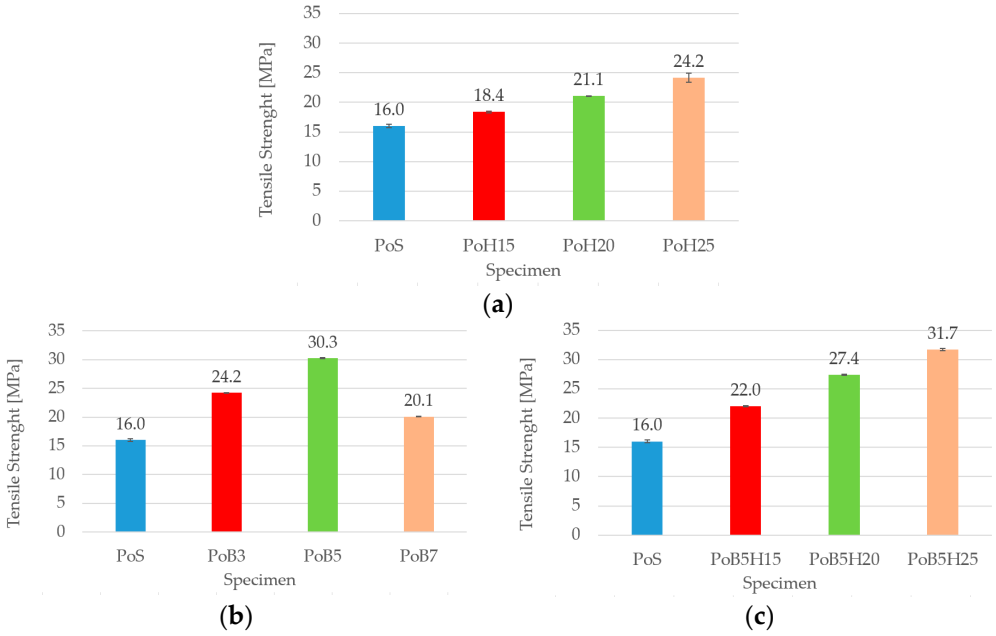

Figure 6. Tensile strength results. (**a**) Polymer/henequen composites (15, 20, and 25%); (**b**) polymer plus (3, 5, and 7%) of bentonite; (**c**) polymer plus 15% henequen and 5% of bentonite; polymer plus 20% henequen and 5% of bentonite; and polymer plus 25% henequen and 5% of bentonite.

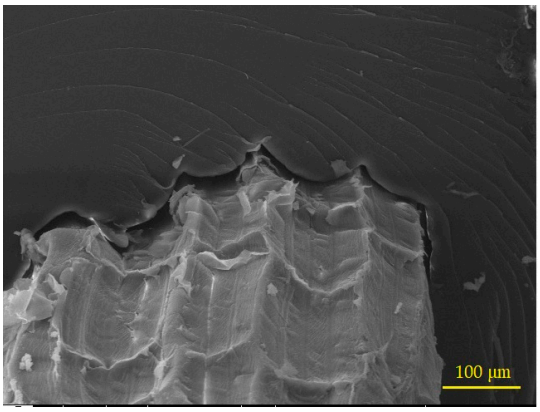

Figure 7. Composite with 15% fiber after tensile test, 350×, bas corresponds to 100 µm.

Increasing the percentage of bentonite in the polymer increases the tensile strength, as presented in Figure 6b. This increment is reversed for a 7% concentration of bentonite due to a partial agglomeration and non-homogeneous distribution of clay particles with an increasing charge concentration that is frequently observed in clay/polymer nanocomposites [36]. In the composites of polymer/bentonite, the clays were treated with quaternary ammonium salt, which allowed the partial exfoliation of the lamellae, provoking a good interaction and distribution between the polymer and the clay. This property manifests itself in the PoB5 composite, in which the best tensile strength result (30.3 MPa) was obtained with an increase of 89% in relation to the pure polymer. In the composite variant PoB7, the agglomeration of the mineral was partial, evidenced by a decrease in the tensile strength of the sample with respect to the PoB3 and PoB5 samples. The suspicion that the agglomeration was partial is corroborated by the fact that the sample with 7% of bentonite still has a greater tensile strength than that of the pure polymer. The addition of 15, 20, and 25% of fiber together with the addition of 5% organophilized bentonite reflects an increase in the tensile values with respect to the respective fiber/polymer compounds, but not with

respect to the combination clay/polymer in which case their values were greater except for the PoH25 sample, as shown in Figure 6c.

The presence of the fiber did not provide a substantial synergistic effect when in the presence of 5% bentonite. This fact can be explained by the appearance of voids in the polymer matrix as seen in the micrographs of Figure 8. These pores of spherical morphology may have been formed by the difficulty in expelling the air caused by the increase in the viscosity of the resin containing clay in the presence of the fibers, in the step of pressing the mold.

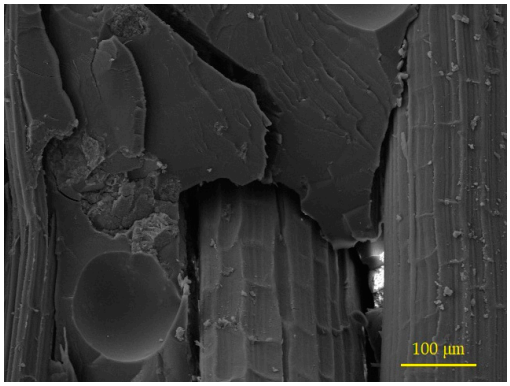

(**a**)

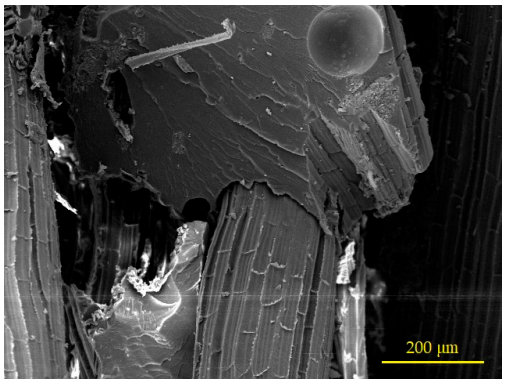

(**b**)

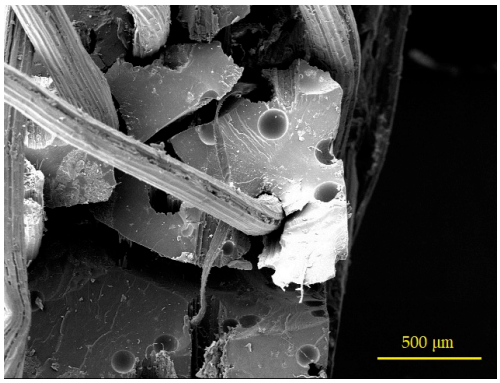

(**c**)

Figure 8. Micrographs of composites polymer/fiber/5% bentonite: (**a**) an amount of 15% fiber, bar corresponds to 100 µm; (**b**) 20% fiber, bar corresponds to 200 µm; and (**c**) 25% fiber, bar corresponds to 500 µm.

Figure 9 shows the transmission electron micrographs of the composite containing 25% fiber and 5%, bentonite (PoB5H25). Observed in Figure 9a are regions where the clay particles are intercalated with polymer and others where the delaminated clay particles (spheres) appear tenuously with a diaphanous appearance, being partially transparent to the electrons, due to their nanometric thickness with little or no stacking. In Figure 9b, regions with interspersed particles and others with particles exfoliated to a greater or lesser degree are observed. Thus, both XRD and TEM, results show that intercalated, partially exfoliated nanocomposites were obtained.

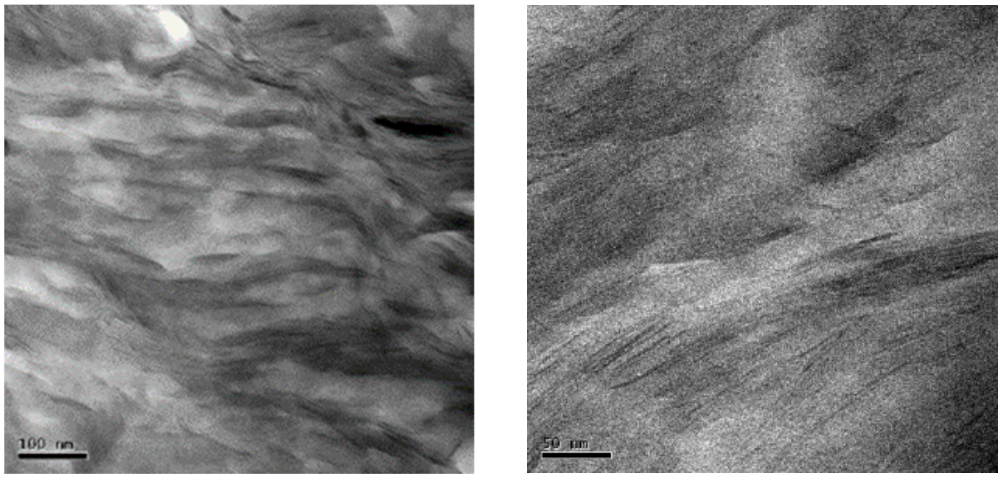

(**a**) (**b**)

Figure 9. Transmission electron micrographs of the PoB5H25 composite: (**a**) increase of 200,000×, (**b**) increase of 400,000×.

The impact resistance analysis showed increases of 146, 161, and 169% with the additions of fibers of 15, 20, and 25%, as presented in Figure 10a. The clay/polymer composites presented less impact resistance than the fiber/polymer composites, as shown in Figure 10a,b. On the other hand, from Figure 10c, we found that the composites PoB5H15 and PoB5H20 had similar values of impact resistance, with a 159% increment with respect to the pure polymer. The composite PoB5H25 had the highest impact strength (2.23 kg-m/cm^2, 219% increase over the pure polymer). Unlike the occurrence in the tensile tests, bentonite had a synergistic effect on the impact strength for each proportion of fiber used, possibly due to the influence of the strain rate in the progression of cracks caused by spherical defects present in the fiber/clay/bentonite composites, as presented in Figure 10b,c.

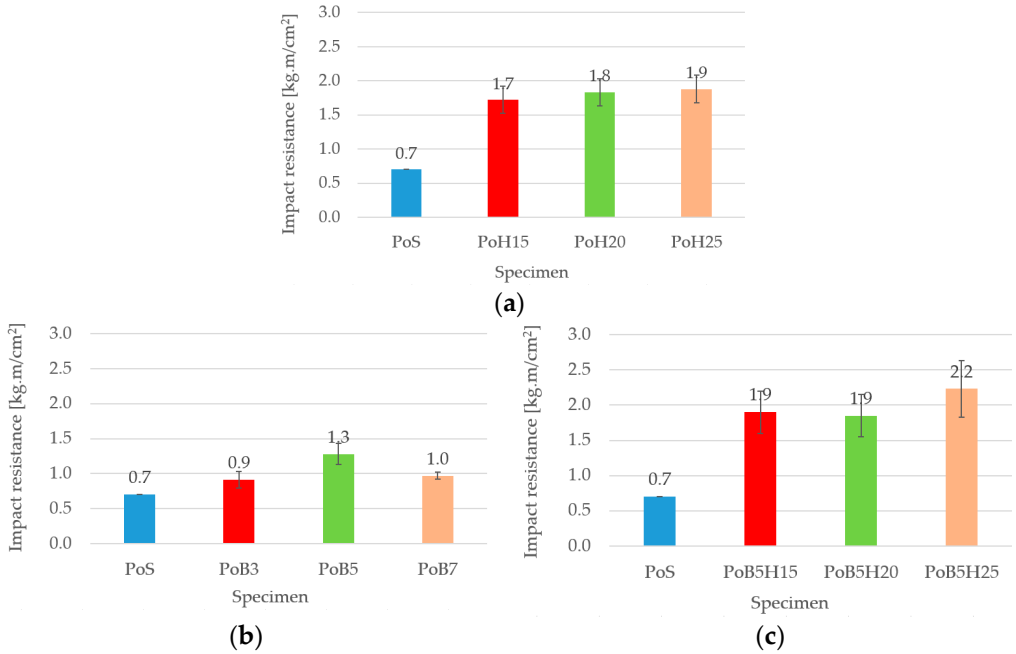

Figure 10. Impact strength of neat polymer: (**a**) polymer plus polymer samples plus 15, 20, and 25% henequen; (**b**) polymer and polymer plus bentonite 3, 5, and 7%, respectively; (**c**) polymer plus 15% henequen and 5% bentonite; polymer plus 20% henequen and 5% bentonite; and polymer plus 25% henequen and 5% bentonite, respectively.

3.2. Computational Model Validation

The proposed and implemented numerical model was validated from the comparison between the experimental and the numerical simulation results. The combination of materials used were PoH15, PoH20, PoB5H15, and PoB5H25. The results are summarized in Table 4, and a comparison was made between the elastic modulus values of the samples. An improvement in the elastic modulus was perceived in the samples with bentonite, where the PoB5H15 and PoB5H20 samples show increases of 45.22% and 26.87%, respectively, compared to the PoH15 and PoH20 samples. This could be attributed to the rigidity of the filler particles, which increases the modulus due to the reinforcing effect [40]. Not so for the PoB5H25 sample, which presented a loss of stiffness of 26.39% compared to PoH25. This behavior occurs in fiber-reinforced polymer matrix composites and is justified by the existence of a limit in the amount of fibers which can begin to optimally cohere the matrix and, when this limit is exceeded, a decrease occurs in the material properties [36,37]. The semi-empirical equations will be applied to hybrid polymer nanocomposites reinforced with similar fibers and clays.

Table 4. Experimental results.

Sample	Endurance (MPa)	Elongation (%)	Elastic Module (MPa)	Increase (%)
PoH15	18.37	9.60	191.35	
PoB5H15	18.34	6.60	277.88	45.22
PoH20	21.06	10.1	208.51	
PoB5H20	20.37	7.70	264.55	26.87
PoH25	24.16	4.50	536.89	
PoB5H25	21.34	5.40	395.19	−26.39

Despite the different collapse loads used, all the samples exhibited similar cracking, propagation, and physical discontinuity behavior. The cracks start at one of the ends of the specimen, because the highest mechanical stress was discovered at the ends. In that way, the crack propagates diagonally, as illustrated in Figure 11.

Figure 11. View of the breakage of the composite material samples.

The fractomechanical behavior is presented from experimental stress–strain graphs (blue color) and although all the samples have the same behavior, Figure 11 presents the stress–strain graph corresponding to 15% of fibers, specifically the PoH15 material, where two zones are seen, one linear elastic and the other softening. The linear elastic zone harbors a higher fracture energy than the softening zone, due to the nature of the properties of the natural fibers in conjunction with the matrix. At the same time, it is possible to

visualize that when the maximum tensile load is exceeded, the total collapse of the material is progressive and not instantaneous like brittle materials. The fibers present a tensile stress of 23.15 N, and maximum tension of 283 MPa.

The constitutive model proposed through the implementation of the calculation algorithm has a good fit concerning the collapse load since the tensional arguments start the criterion of failure or damage, as shown in Figure 12a–d. On the other hand, the loss of mechanical properties, generated by the numerical softening controlled by the internal variable of damage, presents a convincing but not exact fit. Since the proposed algorithm does not contemplate the normalization of the fracture energy in the damage parameter and focuses on a linear damage loss, it is adjusted by the unit deformation at the moment the discontinuity is completed, which is highly sensitive to local deformation at each node and, therefore, to the element that is analyzed at different times.

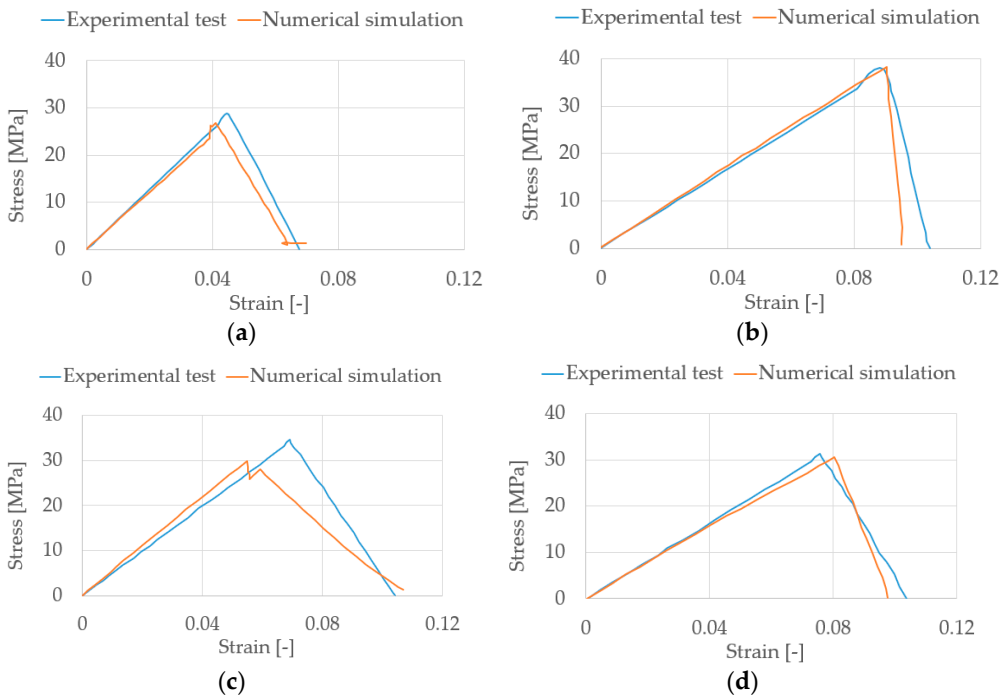

Figure 12. Stress vs. strain in the composite material: (**a**) PoH15; (**b**) PoH20; (**c**) PoB5H15; (**d**) PoB5H25.

The two main contributions of this work are that it was determined that the addition of bentonite nanoparticles, at 5 wt%, previously organophilized, increased the tensile and impact resistance of the polymeric matrix composites (thermoset) reinforced with Cannabis sativa fibers. Likewise, the damage model used (simple to implement and requiring few parameters) allows the simulation of the behavior of these compounds under uniaxial tension, mainly in the area before the tensile limit. This will allow, after its generalization to 2D and 3D, the simulation of parts, parts of machines, and structures, contributing to their design and anticipating failures under loads over time.

4. Conclusions

The polyester resin/henequen fiber-reinforced composites were obtained, showing tensile strength increases of up to approximately 50%, relative to the value obtained with the neat resin. For the resin/clay composites, the tensile strength increased up to 90% and in the resin/fiber/clay composites no synergistic effect was observed with the addition of clay. This lack of synergism can be explained by defects introduced in the resin during the conformation of the resin/fiber/clay composites, due to the increased viscosity of the resin-incorporating clay.

The impact strength increases up to 170% for the polyester resin/fiber composites, relative to the value obtained only with resin, which was higher than those obtained in the polymer/clay composites. For the resin/fiber/clay composites, a synergistic effect was observed when the clay is added in 5%, resulting in an increase in the impact resistance up to 220% as compared with the neat resin.

The elastic modulus increased by 45.22% with the bentonite clay added to the polymer resin/natural fibers.

In this study, a scalar damage model was formulated, implemented, and validated for composite materials reinforced with natural fibers, in three-dimensional solid elements. Each one of the field variables developed in the algorithm was obtained from the constitutive model obtained in the experimental tests. The contrast of the numerical results with those obtained in the experimental tests revealed an adequate correlation between them, and the damage model with tensor arguments presented a collapse load, adjusted to the experimental load. However, it presented a high dispersion in one of the four numerical simulations, with a percentage difference of 12.1%, but in the other three numerical simulations, the largest percentage difference was 6.15% in the collapse load.

The polymer resin/natural fibers/bentonite clay composites obtained have a potential application as masonry structures and structural health monitoring applications, as sustainable materials for construction, as well as electrical insulation.

Author Contributions: Conceptualization, A.R.S.; methodology, G.G.d.P.; software, F.R.V.D.; validation, R.Q.; formal analysis, A.A.A.; investigation, H.F.L.; resources, F.P.R.; data curation, C.G.K.; writing—original draft preparation, M.V.F.; writing—review and editing, M.V.F.; supervision, A.R.S.; project administration, J.L.V.R.; funding acquisition, M.E.F.A. All authors have read and agreed to the published version of the manuscript.

Funding: This research received no external funding.

Institutional Review Board Statement: Not applicable.

Informed Consent Statement: Not applicable.

Data Availability Statement: Data is not publicly available.

Conflicts of Interest: The authors declare no conflict of interest.

References

1. Abdellaoui, H.; Bensalah, H.; Echaabi, J.; Bouhfid, R.; Qaiss, Y.A. Fabrication, characterization and modelling of laminated composites based on woven jute fibres reinforced epoxy resin. *Mater. Des.* **2015**, *68*, 104–113. [CrossRef]
2. Bledzki, A.K.; Gassan, Y.J. Composites reinforced with cellulose based fibres. *Prog. Polym. Sci.* **1999**, *24*, 221–274. [CrossRef]
3. Nam, T.H.; Ogihara, S.; Kobayashi, S.; Goto, Y.K. Effects of surface treatment on mechanical and thermal properties of jute fabric-reinforced poly(butylene succinate) biodegradable composites. *Adv. Compos. Mater.* **2015**, *24*, 161–178. [CrossRef]
4. Herrera-Franco, P.J.; Valadez-González, Y.A. Mechanical properties of continuous natural fibre-reinforced polymer composites. *Compos. Part Appl. Sci. Manuf.* **2004**, *35*, 339–345. [CrossRef]
5. Sanchez, E.M.S.; Cavani, C.S.; Leal, C.V.; Sanchez, Y.C.G. Unsaturated polyester resin composite with sugar cane bagasse: Influence of treatment on the fibers properties. *Polímeros* **2010**, *20*, 194–200. [CrossRef]
6. Silva, R.; Haraguchi, S.K.; Muniz, E.C.; Rubira, Y.A.F. Aplicações de fibras lignocelulósicas na química de polímeros e em compósitos. *Quím. Nova* **2009**, *32*, 661–671. [CrossRef]
7. Rodríguez-Soto, A.-A.; Valín-Rivera, J.-L.; Díaz, D.; Muniz-Fonseca, V.; Sanabio-Alves-Borges, Y.L.-M. Desarrollo de un material compuesto de fibras de henequén utilizando una matriz termofija. *Ing. Mec.* **2014**, *17*, 264–272.
8. Hossen, M.F.; Hamdan, S.; Rahman, M.R.; Rahman, M.M.; Liew, F.K.; Lai, Y.J.C. Effect of fiber treatment and nanoclay on the tensile properties of jute fiber reinforced polyethylene/clay nanocomposites. *Fibers Polym.* **2015**, *16*, 479–485. [CrossRef]
9. Wagh, J.; Madgule, M.; Awadhani, Y.L.V. Investigative studies on the mechanical behavior of Jute, Sisal, Hemp, and glass fiber-based composite material. *Mater. Today Proc.* **2022**. [CrossRef]
10. Hamou, K.B.; Kaddami, H.; Elisabete, F.; Erchiqui, Y.F. Synergistic association of wood /hemp fibers reinforcements on mechanical, physical and thermal properties of polypropylene-based hybrid composites. *Ind. Crop. Prod.* **2023**, *192*, 116052. [CrossRef]
11. Mylsamy, B.; Palaniappan, S.K.; Subramani, S.P.; Pal, S.K.; Sethuraman, Y.B. Innovative characterization and mechanical properties of natural cellulosic Coccinia Indica fiber and its composites. *Mater. Test.* **2020**, *62*, 61–67. [CrossRef]
12. Gudapati, S.P.K.; Krishna, C.V.; Prasad, Y.A.V.R. Effect of nano clay on tensile and flexural properties of vakka fiber polyester composites. *Mater. Today Proc.* **2019**, *18*, 2032–2035. [CrossRef]

13. Ranjith, C.B.; Vasudevan, Y.A. Enhancement on flexural strength of glass fiber composite addition of nano clay and (Mwcnt) using novel C shaped spiral tube position by vacuum bag molding process. *Mater. Today Proc.* **2022**, *69*, 1223–1228. [CrossRef]
14. Alekseeva, O.V.; Noskov, A.V.; Agafonov, Y.A.V. Structure, physicochemical properties, and adsorption performance of the ethyl cellulose/bentonite composite films. *Cellulose* **2022**, *29*, 3947–3961. [CrossRef] [PubMed]
15. Boem, I. Characterization of Textile-Reinforced Mortar: State of the Art and Detail-Level Modeling with a Free Open-Source Finite-Element Code. *J. Compos. Constr.* **2022**, *26*, 4022060. [CrossRef]
16. Nayak, J.R.; Bochen, J.; Gołaszewska, Y.M. Experimental studies on the effect of natural and synthetic fibers on properties of fresh and hardened mortar. *Constr. Build. Mater.* **2022**, *347*, 128550. [CrossRef]
17. Chun, B.; Oh, T.; Jang, Y.S.; Lee, S.K.; Lee, J.-H.; Yoo, Y.D.-Y. Strengthening effect of concrete beams using ultra-rapid-hardening fiber-reinforced mortar under flexure. *Constr. Build. Mater.* **2022**, *352*, 129064. [CrossRef]
18. Silva, G.; Kim, S.; Aguilar, R.; Nakamatsu, Y.J. Natural fibers as reinforcement additives for geopolymers–A review of potential eco-friendly applications to the construction industry. *Sustain. Mater. Technol.* **2020**, *23*, e00132. [CrossRef]
19. Olivito, R.S.; Cevallos, O.A.; Carrozzini, Y.A. Development of durable cementitious composites using sisal and flax fabrics for reinforcement of masonry structures. *Mater. Des.* **2014**, *57*, 258–268. [CrossRef]
20. de Carvalho Bello, C.B.; Boem, I.; Cecchi, A.; Gattesco, N.; Oliveira, Y.D.V. Experimental tests for the characterization of sisal fiber reinforced cementitious matrix for strengthening masonry structures. *Constr. Build. Mater.* **2019**, *219*, 44–55. [CrossRef]
21. Mercedes, L.; Gil, L.; Bernat-Maso, Y.E. Mechanical performance of vegetal fabric reinforced cementitious matrix (FRCM) composites. *Constr. Build. Mater.* **2018**, *175*, 161–173. [CrossRef]
22. Rodríguez-González, J.A.; Renteria-Rodríguez, V.; Rubio-González, C.; Franco-Urquiza, Y.E.A. Spray-coating of graphene nanoplatelets on sisal fibers and its influence on electromechanical behavior of biocomposite laminates. *J. Reinf. Plast. Compos.* **2023**, 07316844231152911. [CrossRef]
23. Murali Mohan Rao, K.; Rao, K.M.; Prasad, Y.A.V.R. Fabrication and testing of natural fibre composites: Vakka, sisal, bamboo and banana. *Mater. Des.* **2010**, *31*, 508–513. [CrossRef]
24. Gu, J.; Li, K.; Su, Y.L. A Continuum Damage Model for Intralaminar Progressive Failure Analysis of CFRP Laminates Based on the Modified Puck's Theory. *Materials* **2019**, *12*, 3292. [CrossRef]
25. Sun, L.; Wang, J.; Hu, H.; Ni, Y.A. A Simplified Computational Strategy Focused on Resin Damage to Study Matrix Cracking of The Cross-Ply Laminates Under Uniaxial Tension Load. *Materials* **2019**, *12*, 1984. [CrossRef]
26. González Del Solar, G.; Martín, P.; Maldonado, Y.N. Formulación, implementación y validación de un modelo de daño escalar para materiales frágiles aplicado a elementos sólidos tridimensionales. *Rev. Ing. Constr.* **2018**, *33*, 111–122. [CrossRef]
27. Rezasefat, M.; Mostafavi, Y.; Ma, D.; Manes, Y.A. A hybrid micro-macro mechanical damage model to consider the influence of resin-rich zones on the transverse tensile behaviour of unidirectional composites. *Compos. Struct.* **2023**, *308*, 116714. [CrossRef]
28. Tijs, B.H.A.H.; Dávila, C.G.; Turon, A.; Bisagni, Y.C. The importance of accounting for large deformation in continuum damage models in predicting matrix failure of composites. *Compos. Part Appl. Sci. Manuf.* **2023**, *164*, 107263. [CrossRef]
29. Fonseca, V.M. Desenvolvimento de Sistema Antichama Aplicado a Compósitos de Poliéster Insaturado Reforçados Com Fibras de Sisal. Tese de Doutorado, Universidade Federal do Rio Grande do Norte, Natal, Brasil, 2002.
30. de Carvalho, L.H.; Cavalcanti, Y.W.S. Propriedades mecânicas de tração de compósitos poliéster/tecidos híbridos sisal/vidro. *Polímeros* **2006**, *16*, 33–37. [CrossRef]
31. Kachanov, L.M. Rupture Time Under Creep Conditions. *Int. J. Fract.* **1999**, *97*, 11–18. [CrossRef]
32. Cervera, M.; Manzoli, O.L.; Oliver, Y.J. A rate-dependent isotropic damage model for the seismic analysis of concrete dams. *Eng. Comput.* **1996**, *25*, 987–1010. [CrossRef]
33. Lubliner, J. *Plasticity Tehory*; Pearson Education, Inc.: New York, NY, USA, 2006.
34. Lemaître, J.; Chaboche, J.Y. Aspect Phenomenologique de la Rupture Par Endommagement. 1978. [En Línea]. Available online: https://www.semanticscholar.org/paper/ASPECT-PHENOMENOLOGIQUE-DE-LA-RUPTURE-PAR-Lema%C3%AEtre-Chaboche/f55030466a796d43727d00769d56a67d9be37372 (accessed on 16 January 2023).
35. Maugin, G.A. *The Thermomechanics of Plasticity and Fracture*; Cambridge University Press: Singapore, 1992.
36. Coleman, B.D.; Gurtin, Y.M.E. Thermodynamics with Internal State Variables. *J. Chem. Phys.* **1967**, *47*, 597–613. [CrossRef]
37. Horstemeyer, M.F.; Bammann, Y.D.J. Historical review of internal state variable theory for inelasticity. *Int. J. Plast.* **2010**, *26*, 1310–1334. [CrossRef]
38. Luo, S.; Netravali, Y.A.N. Characterization of henequen fibers and the henequen fiber/poly(hydroxybutyrate-co-hydroxyvalerate) interface. *J. Adhes. Sci. Technol.* **2001**, *15*, 423–437. [CrossRef]
39. Ku, H.; Wang, H.; Pattarachaiyakoop, N.; Trada, Y.M. A review on the tensile properties of natural fiber reinforced polymer composites. *Compos. Part B Eng.* **2011**, *42*, 856–873. [CrossRef]
40. Mahadeva Raju, G.K.; Dakshayini, B.S.; Madhu, G.M.; Khan, M.A.; Reddy, Y.P.D.S. Characterizing and Modeling of Mechanical Properties of Epoxy Polymer Composites Reinforced with Bentonite Clay. *Mater. Today Proc.* **2018**, *5 Pt 2*, 28098–28107. [CrossRef]